

*XMM-Newton* OBSERVATIONS OF BROAD FEK $\alpha$  EMISSION FROM A SEYFERT 1.9 GALAXY  
MCG-5-23-16

G. C. DEWANGAN, R. E. GRIFFITHS, AND N. J. SCHURCH

Department of Physics, Carnegie Mellon University, 5000 Forbes Ave, Pittsburgh, PA 15213 USA  
gulabd@cmu.edu

*Revision 1, Submitted to ApJ*

ABSTRACT

*XMM-Newton* observations of the bright Seyfert 1.9 galaxy MCG-5-23-16 have revealed a broad FeK $\alpha$  emission line which is nearly symmetric in contrast to the broad and red-shifted asymmetric FeK $\alpha$  line sometimes observed from Seyfert 1 galaxies. The FeK $\alpha$  line has two distinct components – a narrow unresolved component with equivalent width of  $\sim 40$  eV and a broad component with full width at half maximum of  $\sim 40000$  km s $^{-1}$  and equivalent width of  $\sim 120$  eV. An absorption feature at  $\sim 7.1$  keV has also been observed. The energies of the emission and absorption features are consistent with those arising from neutral iron. The broad component is consistent with an FeK $\alpha$  emission line expected from a relativistic accretion disk around a Schwarzschild or a Kerr black hole. Alternatively, most of the flux in the broad component could also be modeled as reflection emission which mimics emission line like feature due to the presence of iron K-shell edge at  $\sim 7.1$  keV, however, the reflection fraction,  $R \sim 3$ , is much higher than that inferred from the *BeppoSAX* observations ( $R \sim 0.5$ ). The disk inclination angle of  $\sim 47$  deg, inferred from the disk-line fits, and the absorption column ( $N_{\text{H}} \sim 10^{22}$  cm $^{-2}$ ), inferred from the low-energy spectral curvature due to photoelectric absorption, suggest that our line of sight passes through the outer edge of a putative torus and are consistent with those expected for a Seyfert 1.9 galaxy falling within the unification scheme. The strength of the narrow iron K $\alpha$  emission and the optical depth of the iron K absorption edge suggest their origin in the putative torus with  $N_{\text{H}} \sim 10^{24}$  cm $^{-2}$  in the inner regions and  $N_{\text{H}} \sim 10^{22}$  cm $^{-2}$  in the outer edges. The strength of the broad component of FeK $\alpha$  varied by a factor of  $\sim 2$  between the two *XMM-Newton* observations taken  $\sim 6$  months apart, while the narrow component of FeK $\alpha$  and the continuum flux did not appear to vary appreciably. There is evidence for a weakening in the strength of the broad iron K $\alpha$  emission with the flattening of the observed continuum. This can perhaps be explained if the shape of the continuum is coupled with the ionization stage of the reflector.

*Subject headings:* Active galactic nuclei: accretion disks — line: formation

1. INTRODUCTION

The Seyfert-type active galactic nuclei (AGNs) appear to be intrinsically X-ray loud and the variation in their X-ray emission is largely due to different absorbing columns along the respective lines of sight. The type 1 and type 2 Seyferts and the intermediate Seyferts (types 1.5, 1.8, and 1.9), all show a similar form in their intrinsic X-ray emission – a power law with photon index of  $\sim 1.9$  which can extend up to a few  $\times 100$  keV, an FeK $\alpha$  line at  $\sim 6.4$  keV, and a reflection hump in the  $\sim 10 - 100$  keV region. However, the obscured Seyferts show a low-energy cut-off of the intrinsic power law due to photoelectric absorption. The exact energy of the cut-off depends on the depth of the absorption column. The obscured Seyferts also show unabsorbed soft X-ray emission composed of a number of photo-excited emission lines (Kinkhabwala et al. 2002; Schurch et al. 2003). This component is often extended, non-variable and cannot be the emission from the accretion disk. X-ray emission arising from the accretion disks of obscured Seyfert galaxies (e.g., the broad iron K $\alpha$  emission) provide us with the opportunity to study the geometry and physical conditions in the inner regions surrounding a super massive black hole (SMBH), thus helping us in understanding the diversity in the AGN characteristics.

The iron K $\alpha$  emission is the most prominent ubiquitous feature in the 2 – 10 keV region of the X-ray spectra of

AGNs. This emission appears to be a general characteristic of AGNs. Complex iron K $\alpha$  emission consisting of multiple components and/or asymmetric profiles arising from neutral and/or ionized iron have been observed from many Seyfert 1 galaxies and provide the strongest evidence for the existence of cold material in the central regions of AGNs. The broad iron K $\alpha$  emission is the key feature in studies of the geometry and nature of the accretion disks around black holes. The line profile can also be used to infer the Schwarzschild or Kerr nature of black holes. While some Seyfert 1 galaxies show broad iron K-shell emission, there are only a few Seyfert 2 galaxies with broad iron K $\alpha$  emission. This is likely due to the difficulty in detecting the broad wings in the presence of large absorbing columns along our line of sight to a type 2 nucleus. The narrow-emission line galaxies (NELGs) are good targets for study of the iron K $\alpha$  emission from the obscured AGNs. Optically, NELGs are the same as Seyfert 2s and show narrow optical emission lines, often with broad wings of H $\alpha$  and P $\beta$  which makes them Seyfert 1.9 nuclei. NELGs are bright and variable X-ray sources which were discovered in early X-ray surveys (Marshall et al. 1979; Griffiths et al. 1978). In this paper, we present a detailed study of the iron K $\alpha$  emission from an obscured Seyfert galaxy MCG-5-23-16 using *XMM-Newton* observations.

MCG-5-23-16 is an S0 galaxy (Ferruit, Wilson, & Mulchaey 2000) first discovered in X-rays by Schnopper et

al. (1978) who also found its' optical spectrum to be that of a narrow emission-line galaxy at a redshift of 0.0083. Veron et al. (1980) classified this galaxy as a Seyfert 1.9 based on the possible presence of a broad component in H $\alpha$ . MCG-5-23-16 with a V-magnitude of 13.7 is one of the brightest Seyfert galaxies in hard X-rays and is also one of the few Seyferts detected at  $\gamma$ -ray energies (Bignami et al. 1979; Pollock et al. 1981). Its 2–10 keV flux, measured to be  $\sim 8 \times 10^{-11}$  erg cm $^{-2}$  s $^{-1}$  in 1978 (Tennant 1983), decreased by a factor of four in 1989 (Nandra & Pounds 1994), and then increased to  $\sim 9 \times 10^{-11}$  erg cm $^{-2}$  s $^{-1}$  in 1996 (Weaver, Krolik, & Pier 1998) before decreasing again to  $7 \times 10^{-11}$  erg cm $^{-2}$  s $^{-1}$  in 2001 (this work). Previous X-ray observations of MCG -5-23-16 showed a highly absorbed X-ray spectrum ( $N_{\text{H}} \sim 10^{22}$  cm $^{-2}$ , Turner & Pounds 1989) and a strong iron K $\alpha$  fluorescence line with equivalent width of 300 – 400 eV (Singh, Rao, & Vahia 1992; Nandra & Pounds 1994; Weaver et al. 1997; Weaver, Krolik, & Pier 1998). Weaver et al. (1997) reported a complex iron K-shell line profile in an *ASCA* observation of this source. These authors discovered a narrow core at the systemic velocity of the galaxy and wings to the red and blue sides of this core. They modeled the line profile with three Gaussian having central energies 5.37, 6.37, and 6.58 keV. Alternatively, the data could also be modeled with a line profile from an accretion disk, superimposed upon a narrow Gaussian profile. These data have provided some of the best evidence to date for contributions from two distinct regions to the observed iron line profile.

In this paper we present the first results from the *XMM-Newton* observations of MCG-5-23-16. The paper is organized as follows. In Sect. 2, we describe the *XMM-Newton* observations and the data selection. In Sect. 3, we present the detailed spectral analysis of the FeK $\alpha$  region. We discuss our results in Sect. 4 followed by conclusions in Sect. 5.

## 2. OBSERVATIONS AND DATA SELECTION

*XMM-Newton* observatory (Jansen et al. 2001) has three Wolter type 1 X-ray telescopes with three European Photon Imaging Cameras (EPICs) – one PN (Strüder et al. 2001) and two MOS CCD (Turner et al. 2001) cameras as the imaging spectrometers. All *XMM-Newton* instruments operate simultaneously. *XMM-Newton* observed MCG-5-23-16 twice on 13 May 2001 and 1 December 2001 for 38ks and 25ks, respectively. The EPIC PN and MOS observations were carried out in the full frame mode using the medium filter. Here we present the data from the PN and MOS cameras.

The raw PN and MOS events were processed and filtered using the most recent updated calibration database and analysis software (SAS v5.3.3) available in December 2002. Events in the bad pixels file and those adjacent pixels were discarded. Events with pattern 0-4 (single and double) for the PN and 0-12 (similar to *ASCA* event grades 0-4) for the MOS cameras were selected for both the observations of 2001. Examination of background light curves extracted from source-free regions showed that both the observations were affected by particle induced flares. These flares are characterized by strong and rapid variability in the background light curve. The particle induced events were filtered out by excluding the time periods where the count rate increased by  $3\sigma$  from the quies-

cent state background rate. This resulted in net exposure times of 8.5ks and 13.1ks for the PN and MOS, respectively for the observation of May 2001. The observation of December 2001 was not affected severely by the particle induced flares: the net exposure times are 19.7ks for the PN and MOS cameras.

The source spectra were extracted from the final filtered event lists using a circular region of radius 90'' centered on the observed position of MCG-5-23-16 for both the PN and MOS cameras. Background spectra were extracted using appropriate annular regions around the observed position of MCG-5-23-16. Any source in the background region was masked out. Appropriate response and effective area files for both the PN and MOS cameras were created using the SAS.

## 3. SPECTRAL ANALYSIS

The PN and MOS spectra of MCG-5-23-16 were analyzed using the spectral fitting package XSPEC v11.2.0. In order to check for consistency in the spectral calibration of PN and MOS cameras, to check for spectral variability and to derive time averaged spectral characteristics of MCG-5-23-16, we have carried out spectral model fitting (i) to the individual PN and MOS data sets extracted from each observation, (ii) jointly to the PN and MOS data sets for each observation, and (iii) to the time averaged PN data obtained by combining the two PN data sets from the two observations. Thus, for spectral fitting, we formed nine data sets from the two observations carried out using the three imaging cameras: PN, MOS1, and MOS2. The nine data sets were first fitted by a simple absorbed power-law model over the entire 0.2 – 12 keV bandpass. None of the fits was acceptable e.g., the power-law fit to the combined PN spectrum resulted in a minimum  $\chi^2$  ( $\chi^2_{min}$ ) of 2503.7 for 504 degrees of freedom (dof). To show the significant deviations from a best-fit power law and to determine the true continuum shape, we refitted the absorbed power-law model after excluding the significant features. For these fits we used the data in the 2.5 – 5 keV and 7.5 – 10 keV bands. In these bands, AGNs usually do not show any significant localized feature. Figure 1 shows the combined PN data fitted with the absorbed power-law model and the ratio of data to the best-fit model extrapolated to lower and higher energies. As can be seen in Fig. 1, the poor fit is due to the significant features: a soft excess component below  $\sim 1$  keV, a strong iron K $\alpha$  emission line at  $\sim 6.4$  keV, and likely excess emission above 10 keV. This paper concentrates on the 2.5 – 12 keV band and the soft X-ray spectrum will be studied in a separate paper using RGS data also.

### 3.1. The 2.5 – 10 keV continuum

To characterize the X-ray continuum, simple red-shifted power-law models modified by absorption due to an intervening medium at  $z = 0$  were fitted to the six spectra derived from the two observations with the three EPIC cameras: PN, MOS1, and MOS2. These fits were carried out over the 2.5 – 10 keV band excluding the FeK $\alpha$  region (5 – 7.5 keV). All the fits resulted in acceptable  $\chi^2$ ; however, the best-fit values of equivalent hydrogen column ( $N_{\text{H}}$ ) were much higher ( $N_{\text{H}} \sim 1.7 \times 10^{22}$  cm $^{-2}$  for the PN data of December 2001) than the Galactic column of

$8.82 \times 10^{20} \text{ cm}^{-2}$  (Elvis, Wilkes, & Lockman 1989). Setting the  $N_{\text{H}}$  parameter to the Galactic value resulted in unacceptable fits for all the data sets, thus implying heavy obscuration. The excess absorption column was then determined by introducing an additional absorption component at the source redshift and by refitting the power-law model to individual data sets. Table 1 lists the best-fit parameters: excess  $N_{\text{H}}$ , the photon index  $\Gamma_X$ , and the fit-statistic  $\chi^2_{\text{min}}$ . All the errors quoted, here and below, are at the 90% confidence level. Also listed in Table 1 are the observed flux in the 2.5 – 10 keV band and the absorption corrected (intrinsic) flux in the same band. As can be seen in Table 1, the best-fit parameters  $N_{\text{H}}$  and  $\Gamma_X$ , derived from the data obtained simultaneously with different instruments, are consistent within the errors. However, the observed flux is found to differ by  $\sim 20\%$  between EPIC PN and MOS cameras. This discrepancy is not unusual for X-ray instruments in their early phase of calibration.

In order to further constrain the spectral shape, the absorbed power-law model was fitted to the PN and MOS spectra jointly. The relative normalizations for the different instruments were kept free allowing for the small difference in the calibrated absolute flux, and any differences in the fraction of encircled counts contained in the PN and MOS extraction cells. The results of these fits are also listed in Table 1. There are small variations in the best-fit spectral parameters between the two observations:  $\Delta N_{\text{H}} = (4.4 \pm 2.7) \times 10^{21} \text{ cm}^{-2}$ ;  $\Delta \Gamma_X = 0.13 \pm 0.06$ ;  $\Delta f_{\text{int}} = 7 \times 10^{-12} \text{ erg s}^{-1} \text{ cm}^{-2}$ . The source became harder and fainter in Dec. 2001.

To determine the average continuum shape, we fitted the absorbed and red-shifted power-law model to the time averaged PN data obtained by combining the two PN data sets from the two observations. The time averaged photon index is  $\Gamma_X = 1.69 \pm 0.03$  and the observed flux in the 2.5 – 10 keV band is  $7 \times 10^{-11} \text{ erg s}^{-1} \text{ cm}^{-2}$ .

### 3.2. The iron $K\alpha$ emission

Figure 2 shows the ratio of the PN spectrum extracted from the December 2001 observation to the best-fit power law derived by using the data in the 2.5 – 5 keV and 7.5 – 10 keV bands as described in the preceding section (see Table 1). This plot clearly reveals a broad emission feature in the 5 – 7 keV band and peaking at  $\sim 6.4$  keV. This feature is common among Seyfert galaxies and is attributed to the fluorescence emission from the iron K-shell (e.g., Nandra et al. 1997). The  $\text{Fe}K\alpha$  emission of MCG-5-23-16 appears to be nearly symmetric in its red and blue wings and is clearly different in shape from the red-shifted and asymmetric  $\text{Fe}K\alpha$  profiles generally observed from Seyfert 1 galaxies. Fig. 2 also suggests the likely presence of an iron K-edge at  $\sim 7.1$  keV. To measure the strength and shape of the  $\text{Fe}K\alpha$  emission, we parameterize the observed profile in terms of simple Gaussian models. For this analysis, the co-added PN data were used, as the PN has the largest effective area among the three EPIC cameras. Hence the derived parameters characterize the time averaged  $\text{Fe}K\alpha$  profile. Initially, a narrow unresolved Gaussian ( $\sigma = 0.01$  keV) was used for the  $\text{Fe}K\alpha$  emission and the absorbed and red-shifted power-law model was used for the continuum as described in section 3.1 (Table 1). This model resulted in a poor fit with  $\chi^2_{\text{min}}$  of

262 for 235 dof. The ratio of the data to the best-fit narrow Gaussian model is plotted in Figure 3 (second panel from the top) which shows a dip at  $\sim 6.4$  keV and excess counts on the red and blue sides of the dip. This suggests a strong core at  $\sim 6.4$  keV and broad wings on both sides of the core. Varying the width of the Gaussian improved the fit significantly ( $\Delta\chi^2 = 49$  for 1 additional parameter). This suggests that the line may be broad. Addition of a narrow Gaussian component ( $\sigma = 0.01$  keV) at  $\sim 6.4$  keV improves the fit significantly ( $\Delta\chi^2 = 26.3$  for two additional parameters). The best-fit parameters describing the observed  $\text{Fe}K\alpha$  profile are listed in Table 2. The peak energies of both the narrow and broad components are consistent with neutral iron. The full width at half maximum (FWHM) of the broad component is  $\sim 42000 \text{ km s}^{-1}$ . Addition of an absorption edge at 7.1 keV results in marginal improvement in the fit ( $\Delta\chi^2 = 2.7$  for one additional parameter) at a significance level of  $\sim 93\%$  based on an F-test (Bevington 1969).

The width of the broad iron  $K\alpha$  line observed from MCG-5-23-16 is too large to be produced in regions other than the accretion disk around a super-massive black hole (SMBH). Therefore we checked whether the observed profile is consistent with a relativistic disk-line model (Fabian et al. 1989). This model assumes a Schwarzschild geometry and the disk emissivity is a power-law function of disk radius i.e.  $\propto r^q$ . We fixed the inner disk radius at  $6r_g$  and the outer disk radius at  $500r_g$ , where  $r_g = GM/c^2$ . First we fitted the disk-line model without a narrow Gaussian component. The continuum was the absorbed power-law model as before. The free parameters were the disk inclination angle ( $i$ ) between our line of sight and the disk normal, the disk emissivity  $q$ , and the normalization of the disk line. This fit resulted in an acceptable fit statistic ( $\chi^2_{\text{min}} = 229.8$  for 236 dof). The ratio of the data and the best-fit model is plotted in Figure f4 (top panel). The dip seen at  $\sim 6.4$  keV is due to the characteristic shape of the line profile from a face-on disk – namely a strong core and a red wing. The disk inclination angle was found to be in the range  $0^\circ - 11^\circ$ . This is physically inconsistent with a Seyfert 1.9 galaxy according to the standard unification scheme of Seyfert galaxies (Antonucci 1993). In view of the fact that the observed  $\text{Fe}K\alpha$  profile can be described by a combination of narrow and broad Gaussian and a narrow component is expected due to reflection from cold matter away from the disk, we added a narrow Gaussian component to our disk-line model. The energy of the narrow component was fixed at 6.4 keV. This fit resulted in significant improvement over that without a narrow component ( $\Delta\chi^2 = 32.4$  for one additional parameter). This is an improvement at a significance level of  $> 99.99\%$ . The ratio of the data to the best-fit model is shown in Figure 4 (second panel from the top). The best-fit inclination angle now is  $i = 46.3^{+3.4}_{-3.8}$ . The equivalent width of the disk-line is  $129^{+31}_{-23}$  eV and the line energy is consistent with neutral iron. Addition of an absorption edge at 7.1 keV does not lead to a significant improvement in the fit, and the upper limit to the optical depth is found to be  $\tau < 0.03$ .

We have also tested the observed iron  $K\alpha$  emission profile of MCG-5-23-16 against that expected from an accretion disk around a rotating (Kerr) black hole (Laor 1991). We fixed the inner radius at  $1.23r_g$ , the minimum ra-

dus allowed for a Kerr black hole, and outer radius at  $400r_g$  which is the maximum radius allowed by the model. As before, the disk emissivity is a power-law in radius ( $\propto r^{-q}$ ). The variable parameters were  $E_{FeK\alpha}$ ,  $i$ ,  $q$ , and the line normalization. We used an absorbed and redshifted power-law model for the continuum. The bottom two panels in Fig. 4 show the ratio of the data and best-fit disk-line models for a Kerr black hole. Without a narrow Gaussian component, the fit is acceptable ( $\chi^2 = 251.7$  for 235 dof) but the best-fit inclination angle is  $\sim 18$  deg. Inclusion of a narrow Gaussian component ( $\sigma = 0.01$  keV) resulted in a significant improvement ( $\Delta\chi^2 = 60.5$  for one additional parameter) and in the best-fit inclination angle of  $\sim 47.4$  deg (see Table 2). Addition of an absorption edge at 7.1 keV does not improve the fit significantly ( $\Delta\chi^2 = 0.9$  for one additional dof).

In Figure 5, we have plotted the final best-fit models for the observed iron  $K\alpha$  line profile of MCG-5-23-16. The three models – (i) a combination of a narrow Gaussian and broad Gaussian, (ii) a disk line for a Schwarzschild or (iii) a Kerr black hole all describe the observed data equally well.

In order to look for any variations in the strength of the  $FeK\alpha$  emission, we have also analyzed the observed  $FeK\alpha$  profiles from the two XMM-Newton observations. We used both PN and MOS data for this purpose. We fitted a combination of a broad and a narrow Gaussian profile to the PN and MOS data jointly for each observation. The 2.5 – 10 keV continuum was fixed as determined earlier (see Table 1). The rest-frame line energies of both the narrow and broad components were fixed at 6.4 keV. The results of these fits are listed in Table 3 for both the observations. It appears that the strength of the broad component of the  $FeK\alpha$  line decreased by about a factor of two between the two observations taken six months apart, while the narrow component did not vary significantly.

### 3.3. The Compton reflection model

Under certain conditions, the Compton reflection emission can be important even below  $\sim 10$  keV (see section 4.2). If the onset of the reflection component is at 5 keV, the presence of a strong Fe K-shell edge at  $\sim 7.1$  keV may artificially mimic a broad emission line feature at  $\sim 6.4$  keV. This artificial “broad line” is likely to arise if the observed continuum is flatter and is dominated by the reflection component. The 2.5 – 10 keV photon index of MCG-5-23-16 derived from the combined PN data ( $\Gamma_X \sim 1.7$ ) is flatter than the average 2 – 10 keV photon index of Seyfert galaxies ( $\langle \Gamma_X \rangle \sim 1.9$ ; Mushotzky 1997). This flatter spectrum and strong iron  $K\alpha$  line of MCG-5-23-16 could then be partly due to the contribution of a Compton reflection process in a geometry where the primary X-ray source is partially covered by cold matter e.g. a torus. The reflection emission has been detected from MCG-5-23-16 with RXTE observations in 1995 (Weaver, Krolik, & Pier 1998). To test whether the broad feature near 6.4 keV could be due to reflection and iron K-edge absorption of the primary emission, we have fitted a Compton reflection model to the combined PN data in the 2.5 – 12 keV band. We used the reflection model “pexrav” (Magdziarz & Zdziarski 1995) available with XSPEC. This model calculates the reflected spectrum from a neutral disk

exposed to an exponentially cut-off power-law spectrum (Magdziarz & Zdziarski 1995). Since XMM-Newton does not cover the expected peak ( $\sim 30 - 40$  keV) of the reflection component, it is not possible to constrain all the parameters of the reflection model using XMM-Newton data alone. Instead we fix the cut-off energy of the primary power-law at 200 keV, disk inclination at 50 deg, and the abundance of heavy elements at the solar value. The free parameters are the photon index of the primary power-law, the power-law normalization, and the relative amount of reflection compared to the directly viewed primary spectrum ( $R$ ). We also included a narrow Gaussian line model to describe the  $FeK\alpha$  emission. The results of this fit are listed in Table 4. The best-fit photon index of the incident power-law continuum is  $\sim 1.8$  and is consistent with the mean photon index for Seyfert 1 galaxies. The ratio of the observed data to the best-fit model is shown in Figure 6. Although the fit is acceptable ( $\chi^2_{min} = 224.4$  for 269 dof), there is weak excess emission near 6 keV suggestive of the possible presence of a weak broad emission line. To investigate further, we included an additional Gaussian component in our reflection model and carried out the fitting. This resulted in an improvement in the fit ( $\Delta\chi^2 = 20.1$  at the cost of 2 dof). This is an improvement at a significance level of 99% according to the maximum likelihood test. The best-fit parameters are listed in Table 4. The relative normalization of the reflection emission derived from the PN data is much higher than the value of  $R = 0.54^{+0.26}_{-0.17}$  inferred from the BeppoSAX observations of MCG-5-23-16 (Risaliti 2002). This is due to the excess emission above  $\sim 10$  keV which amounts  $\sim 20\%$  above 10 keV (see Fig. 1). Such a large discrepancy in the reflection emission inferred from the PN and BeppoSAX data could be due to calibration uncertainties. This view is supported by MOS data, albeit lower signal-to-noise, which do not show a clear excess emission above 10 keV.

To test the reliability of the excess emission above 10 keV in the XMM-Newton PN data, we have analyzed the EPIC PN spectrum of a well known BL Lac, Mkn 421. The BL Lac type AGNs do not show the Compton reflection component, just a smooth continuum. Therefore, they are good targets to check the reliability of spectral features in other AGN X-ray spectra. We retrieved the data corresponding to the XMM-Newton observation of Mkn 421 on 4 May 2002 for an exposure time of  $\sim 40$  ks from the public archive maintained at HEASARC. The data were processed in a similar way as described above for MCG-5-23-16. The source spectrum was extracted from an annular region with inner and outer radii of  $10''$  and  $80''$ , respectively and centered at the observed source position. Due to the high flux of Mkn 421, the events from the core of the point spread function were excluded to avoid possible pile-up which results in artificial hardening of the spectrum. The background spectrum was extracted from the source free regions near the position of Mkn 421. New response files were created for Mkn 421. The PN spectrum was then grouped appropriately and fitted by an absorbed power law model in the 2.5 – 10 keV band. Figure 7 shows the PN spectrum of Mkn 421 fitted with a power-law and the ratio of data and the best-fit power-law model. An excess over the best-fit power-law is seen above 10 keV. This excess is  $\sim 20 - 30\%$  above  $\sim 10$  keV which is similar

to that seen in the PN spectrum of MCG-5-23-16 (Fig. 1). Since Mkn 421, being a blazar, is not expected to show any excess emission, we conclude that the excess emission over the power-law seen above  $\sim 10$  keV in the spectra of Mkn 421 and MCG-5-23-16 is likely an artifact and reflects poor spectral calibration of the PN above 10 keV. Lack of any significant feature in the 2.5 – 10 keV band of the Mkn 421 PN spectrum suggests that the spectral calibration of PN in that energy band is indeed good and the presence of a broad iron  $K\alpha$  emission is not an artifact.

We refitted the Compton reflection model to the combined PN data after excluding the data above 10 keV. We utilized the best-fit parameters for the reflection component derived from the *BeppoSAX* observations by Risaliti (2002) and fixed the cut-off energy  $E_C$  at 157 keV and relative normalization  $R$  at 0.54. The best-fit parameters are listed in Table 4. It is clear that a narrow Gaussian and reflection emission cannot account for the strength of the broad feature at  $\sim 6.4$  keV which implies the presence of a broad  $FeK\alpha$  line.

#### 4. DISCUSSION

We have presented the results from the two observations of MCG-5-23-16 using *XMM-Newton*. The 2 – 10 keV flux is found to be  $6.5 \times 10^{-11}$  erg  $s^{-1}$   $cm^{-2}$  during December 2001 and  $7 \times 10^{-11}$  erg  $s^{-1}$   $cm^{-2}$  during the June 2001 observation, comparable with the  $7.3 \times 10^{-11}$  erg  $s^{-1}$   $cm^{-2}$  measured during the *ASCA* observations of 1994 (Weaver et al. 1997). The 2.5 – 10 keV photon index appears to have flattened slightly from  $1.77^{+0.04}_{-0.05}$  (May 2001) to  $1.64^{+0.03}_{-0.03}$  (December 2001). Both these photon indices are steeper than the index of 1.4 – 1.5 observed with *Gingaw* when the source was in a lower flux state (Nandra & Pounds 1994; Smith & Done 1996). The X-ray spectrum of December 2001 is slight flatter than the *ASCA* spectrum of 1994 when the source flux was slightly higher. These observations suggest that the X-ray spectrum flattens at lower flux levels – a general trend well established for Seyfert galaxies (Singh, Rao, & Vahia 1991; Done, Madejski, & Zdotycki 2000; Zdziarski & Grandi 2001; Vaughan & Edelson 2001; Nandra 2001; Dewangan et al. 2002).

##### 4.1. $FeK\alpha$ emission and its variability

*XMM-Newton* observations of MCG-5-23-16 have reaffirmed the presence of a complex iron  $K\alpha$  emission earlier observed with *ASCA* (Weaver et al. 1997; Weaver & Reynolds 1998; Turner, George, Nandra, & Mushotzky 1998) and *RXTE* (Weaver, Krolik, & Pier 1998). Our spectral fits imply that the line is broad, superimposed with a narrow unresolved component, and possibly affected by an absorption edge of iron at 7.1 keV. The width of the broad line derived by fitting a Gaussian profile suggests that this component could only be formed in an accretion disk around a black hole. Indeed the broad component is consistent with that expected from a relativistic accretion disk around a Schwarzschild or a Kerr black hole. Our results also confirm the *ASCA* result that it is difficult to explain the entire line profile as originating entirely in an accretion disk. The Gaussian and relativistic line model fits to the iron  $K\alpha$  line imply two distinct components. The narrow component is unresolved (FWHM  $\lesssim 1000$  km  $s^{-1}$ ) and has an equivalent width of  $\sim 40$  eV.

Similar narrow unresolved components have been observed with *Chandra* and *XMM-Newton* from a number of AGNs (e.g., Kaspi et al. 2001; Pounds et al. 2001; Turner et al. 2002), and are found to have their peak energy at 6.4 keV with equivalent widths of  $\sim 50$  eV. Such narrow components are naturally expected from the torus and/or the broad line region in the framework of the unification model of Seyfert galaxies. The maximum equivalent width of an  $FeK\alpha$  line produced by fluorescence in a cold reflector far from the disk with  $N_H \simeq 10^{23}$   $cm^{-2}$  is  $\simeq 65$  eV in the case of NGC 4258 (Reynolds, Nowak, & Maloney 2000). Thus the observed equivalent width of the narrow iron  $F\alpha$  line of MCG-5-23-16 is consistent with that expected from the torus.

The broad component has an FWHM of  $\sim 4 \times 10^4$  km  $s^{-1}$  and an equivalent width of  $\sim 110$  eV. This component is described by a broad Gaussian or relativistic disk-line arising from an accretion disk around a Schwarzschild or Kerr black hole suggesting that the line profile is not strongly modified by gravitational effects but broadened by the Doppler effect in a rotating disk. The disk-line fits imply that the disk is neutral and the disk-normal is inclined at an angle of  $\sim 50$  deg. The likely presence of an absorption edge at  $\sim 7.1$  keV (see Fig. 2) also suggests that the disk is neutral. The best-fit values of the emissivity indices inferred from the disk-line fits (in Schwarzschild and Kerr geometry) are similar but lower than the average value of 2.5 obtained for Seyfert 1 galaxies (Nandra et al. 1997). It should be noted that Nandra et al. had also fixed the inner radii to  $6r_g$  (Schwarzschild black hole) and  $1.23r_g$  (Kerr black hole). Weaver et al. (1997) inferred  $q$  to be in the range of 5 – 10 but allowed  $r_i$  to vary with the best-fit values in the range 9 – 22. These results imply that if the emissivity law for MCG-5-23-16 is the same as that of an average Seyfert 1 galaxy, then the inner radius of the accretion disk is larger for MCG-5-23-16.

Our spectral fits suggest that the 2.5–10 keV continuum has flattened from  $\Gamma_X \sim 1.77$  (May 2001) to  $\Gamma_X \sim 1.67$  (December 2001) and the broad component of the iron  $K\alpha$  line has weakened from an equivalent width of  $\sim 180$  eV (May 2001) to  $\sim 90$  eV (December 2001). In the *ASCA* observations of May 1991, the photon index and the equivalent width of the broad component of the iron  $K\alpha$  line were found to be  $1.79 \pm 0.08$  and  $254^{+55}_{-77}$ , respectively. These results suggest weakening of the broad iron  $K\alpha$  line with flattening of the X-ray continuum. Higher equivalent widths of the iron  $K\alpha$  emission could be produced by an increased abundance of iron or by increasing the reflection component. It is unlikely that the change in the equivalent width of iron  $K\alpha$  is due to a change in the iron abundance due to the following reasons: (i) it is very unlikely that iron abundance changes by a factor of about two in just six months, and (ii) it is difficult to explain the variation in the shape of the non-thermal X-ray continuum by changing the iron abundance. Increasing the reflection emission from a neutral disk may flatten the continuum. This will require a change in the geometry of the accretion disk-corona system (e.g. increasing the covering factor at the corona will result in more reflection emission). However, this will increase the equivalent width of the iron  $K\alpha$  line with flattening of the contin-

uum. Large equivalent widths of FeK $\alpha$  can be produced if the accretion disk is ionized (Weaver et al. 1997). Dewangan (2002) reported a correlation between the shape of the X-ray spectrum and the energy of the FeK $\alpha$  line among radio-quiet type 1 AGNs and suggested that the accretion disks of AGNs with steeper continua are more ionized. The trend in  $\Gamma_X$  and the equivalent width of iron K $\alpha$  emission from MCG-5-23-16 could be understood if the shape of the X-ray continuum is coupled with the ionization stage of the disk material in MCG-5-23-16 in a similar way to that observed among the radio-quiet AGNs.

#### 4.2. Is the broad feature at $\sim 6.4$ keV really an iron K $\alpha$ line from an accretion disk?

As shown in section 3, the broad feature at 6.4 keV can be modeled as a broad Gaussian (FWHM  $\sim 40000$  km s $^{-1}$ ) or a line profile arising from an accretion disk around a Schwarzschild or a Kerr black hole. Alternatively, most of the flux in the broad component can also be accounted by reflection emission. However, the derived reflection fraction ( $R \sim 3$ ) is much larger than that inferred from the *BeppoSAX* observations of MCG-5-23-16 ( $R \sim 0.5$ ; Risaliti (2002)) and the average value for Seyfert 1 galaxies ( $R \sim 1$ ; Perola et al. 2002). This is not entirely impossible if the reflector is a putative torus far away from the central continuum source. The reflection fraction can be large if the central source was brighter before a time period which is equal to the time delay between the reflected and primary X-ray emission. However, such a large reflection fraction for MCG-5-23-16 is unlikely due to the following reasons – (i) the calibration of the EPIC PN above 10 keV is reliable at a level of  $\sim 20\%$  (Snowden, private communication). MOS data do not show clear excess emission above 10 keV as is the case for PN. (ii) The broad feature at  $\sim 6.4$  keV weakens with flattening of the continuum. This is not expected if the broad feature were the reflection emission. Simultaneous observations with *XMM-Newton* and *Integral* would be crucial to characterize both the FeK $\alpha$  emission and reflection component.

#### 4.3. The Iron K-shell Edge

*XMM-Newton* observations of December 2001 have revealed the presence of an Iron K-shell absorption edge near  $\sim 7.1$  keV. However, the edge is not well constrained and is detected only at a significance level of 93%. The edge energy is not well determined but it appears to be  $\sim 7.1$  keV (see Fig. 2). The optical depth is found to be  $0.03^{+0.04}_{-0.02}$ . Assuming that the edge arises due to the K-shell absorption of neutral iron and the corresponding photoionization cross section ( $2.6 \times 10^{-20}$  cm $^{-2}$ ; Donnelly, Bell, Scott, & Keenan 2000), we determine the column density of neutral iron to be  $N_{\text{Fe}} \approx 1.1 \times 10^{18}$  cm $^{-2}$ . This corresponds to an effective Hydrogen column density of  $N_{\text{H}} \approx 4 \times 10^{22}$  cm $^{-2}$ , which is a factor of two higher than the hydrogen column density derived by fitting an absorbed power-law model to the observed data. Given the uncertainty in the derived value of the optical depth, it cannot be ruled out that the Fe K-edge arises entirely in the absorbing material along our line of sight in the form of a putative torus. It is interesting to investigate whether both the absorption K-edge and the narrow component of the K $\alpha$  line due to iron could be produced in the the putative torus around an accretion

disk. In the case of isotropic emission, the equivalent width of the emission line should be  $\sim 64 f_c N_{\text{H}} A_{\text{Fe}} \times 10^{-23}$ . For a typical covering factor  $f_c \sim 0.7$  for the torus and solar abundances ( $A_{\text{Fe}} = 1$ ), the absorption column required to produce an equivalent width of 40 eV for the narrow iron K $\alpha$  line is  $\sim 10^{23}$  cm $^{-2}$ . This column is larger by a factor of five than the absorption column derived from the power-law fit. It is also larger by about a factor of three than the absorption column derived from the iron K-edge, since the absorption features are produced only by a column along our line of sight while the emission features are spatially integrated in the case of a source which is unresolved. The above results imply that we are viewing the outer edge of a putative torus where the column density is lower than the inner regions of the torus. This is consistent with that expected for a Seyfert 1.9 galaxy from the unification scheme (Antonucci 1993).

## 5. CONCLUSIONS

We studied the 2.5 – 10 keV spectrum of MCG-5-23-16 which was observed twice with *XMM-Newton* in May and December 2001. Our main results are as follows.

1. The iron K $\alpha$  line profile of MCG-5-23-16 is broad and nearly symmetric. The observed profile could be modeled by a combination of a narrow (unresolved) and a broad Gaussian component. The broad component is also consistent with that expected from an accretion disk around a Schwarzschild or a Kerr black hole.
2. The disk inclination angle of  $\sim 46^\circ$ , inferred from the disk-line fits, is consistent with that expected for a Seyfert 1.9 galaxy according to the Seyfert unification picture.
3. Alternatively, most of the flux of the broad feature at 6.4 keV can also be modeled as the reflection emission, however, the reflection fraction ( $\sim 3$ ) is much larger than that derived from the *BeppoSAX* observations ( $R \sim 0.5$ ). This is likely to be due to uncertainty in the calibration of EPIC PN above 10 keV.
4. We have derived three values of absorption column (i)  $N_{\text{H}} \sim 10^{22}$  cm $^{-2}$  from the best-fit absorbed and red shifted power-law model, (ii)  $N_{\text{H}} \sim 4 \times 10^{22}$  cm $^{-2}$  from the absorption edge, and (iii)  $N_{\text{H}} \sim 10^{23}$  cm $^{-2}$  required to produce the narrow iron K $\alpha$  line emission. The above three values are consistent with a geometrical picture in which our line of sight passes through the outer edges of a putative cold torus obscuring the nuclear X-ray source as expected for a Seyfert 1.9 galaxy from the unification scheme.
5. The broad iron K $\alpha$  emission appears to weaken with the flattening of the X-ray continuum. This can be understood if the degree of ionization of iron in the accretion disk decreases with flattening in the X-ray spectrum. However, in any case the disk does not appear to be highly ionized (i.e. Hydrogen or Helium-like iron).

This work is based on observations obtained with *XMM-Newton*, an ESA science mission with instruments and contributions directly funded by ESA member states and the USA (NASA). The authors thank the referee of this paper,

Dr. Kim Weaver, for her comments and suggestions. REG acknowledges NASA award NAG5-9902 in support of his Mission Scientist position on *XMM-Newton*.

## REFERENCES

- Antonucci, R. 1993, *ARA&A*, 31, 473  
 Bevington, P. R. 1969, New York: McGraw-Hill, 1969,  
 Bignami, G. F., Fichtel, C. E., Hartman, R. C., & Thompson, D. J. 1979, *ApJ*, 232, 649  
 Dewangan, G. C., Boller, T., Singh, K. P., & Leighly, K. M. 2002, *A&A*, 390, 65  
 Dewangan, G. C. 2002, *ApJ*, in press.  
 Done, C., Madejski, G. M., & Zdotycki, P. T. 2000, *ApJ*, 536, 213  
 Donnelly, D. W., Bell, K. L., Scott, M. P., & Keenan, F. P. 2000, *ApJ*, 531, 1168  
 Ferruit, P., Wilson, A. S., & Mulchaey, J. 2000, *ApJS*, 128, 139  
 Elvis, M., Wilkes, B. J., & Lockman, F. J. 1989, *AJ*, 97, 777  
 Fabian, A. C., Rees, M. J., Stella, L., & White, N. E. 1989, *MNRAS*, 238, 729  
 George, I. M. & Fabian, A. C. 1991, *MNRAS*, 249, 352  
 Gondoin, P., Orr, A., Lumb, D., & Santos-Lleo, M. 2002, *A&A*, 388, 74  
 Griffiths, R. E., Bradt, H., Briel, U., Doxsey, R. E., Johnston, M., Schwartz, D. A., & Schwarz, J. 1978, *BAAS*, 10, 503  
 Haardt, F. & Maraschi, L. 1993, *ApJ*, 413, 507  
 Jansen, F. et al. 2001, *A&A*, 365, L1  
 Kaspi, S. et al. 2001, *ApJ*, 554, 216  
 Kinkhabwala, A. et al. 2002, *ApJ*, 575, 732  
 Laor, A. 1991, *ApJ*, 376, 90  
 Lightman, A. P. & White, T. R. 1988, *ApJ*, 335, 57  
 Magdziarz, P. & Zdziarski, A. A. 1995, *MNRAS*, 273, 837  
 Marshall, F. E., Boldt, E. A., Holt, S. S., Mushotzky, R. F., Rothschild, R. E., Serlemitsos, P. J., & Pravdo, S. H. 1979, *ApJS*, 40, 657  
 Mushotzky, R. F. 1997, *ASP Conf. Ser.* 128: Mass Ejection from Active Galactic Nuclei, 141  
 Nandra, K. & Pounds, K. A. 1994, *MNRAS*, 268, 405  
 Nandra, K., George, I. M., Mushotzky, R. F., Turner, T. J., & Yaqoob, T. 1997, *ApJ*, 477, 602  
 Nandra, K. 2001, *Advances in Space Research*, 28, 295  
 Perola, G. C., Matt, G., Cappi, M., Fiore, F., Guainazzi, M., Maraschi, L., Petrucci, P. O., & Piro, L. 2002, *A&A*, 389, 802  
 Pollock, A. M. T., Masnou, J. L., Bignami, G. F., Hermsen, W., Swanenburg, B. N., Kanbach, G., Lichti, G. G., & Wills, R. D. 1981, *A&A*, 94, 116  
 Pounds, K., Reeves, J., O'Brien, P., Page, K., Turner, M., & Nayakshin, S. 2001, *ApJ*, 559, 181  
 Reynolds, C. S. & Fabian, A. C. 1997, *MNRAS*, 290, L1  
 Reynolds, C. S. 1999, *ASP Conf. Ser.* 161: High Energy Processes in Accreting Black Holes, 178  
 Reynolds, C. S., Nowak, M. A., & Maloney, P. R. 2000, *ApJ*, 540, 143  
 Reynolds, C. S. 2001, *ASP Conf. Ser.* 224: Probing the Physics of Active Galactic Nuclei, 105  
 Risaliti, G. 2002, *A&A*, 386, 379  
 Schnopper, H. W., Davis, M., Delvaile, J. P., Geller, M. J., & Huchra, J. P. 1978, *Nature*, 275, 719  
 Schurch, N. J., Warwick, R. S., Griffiths, R. E., Ptak, A. F. 2003, *In press*.  
 Singh, K. P., Rao, A. R., & Vahia, M. N. 1991, *A&A*, 248, 37  
 Singh, K. P., Rao, A. R., & Vahia, M. N. 1992, *ApJ*, 385, 132  
 Smith, D. A. & Done, C. 1996, *MNRAS*, 280, 355  
 Strüder, L. et al. 2001, *A&A*, 365, L18  
 Tanaka, Y. et al. 1995, *Nature*, 375, 659  
 Tennant, A. F. 1983, Ph.D. Thesis,  
 Turner, T. J. & Pounds, K. A. 1989, *MNRAS*, 240, 833  
 Turner, T. J., George, I. M., Nandra, K., & Mushotzky, R. F. 1998, *ApJ*, 493, 91  
 Turner, M. J. L. et al. 2001, *A&A*, 365, L27  
 Turner, T. J. et al. 2002, *ApJ*, 574, L123  
 Weaver, K. A., Yaqoob, T., Mushotzky, R. F., Nousek, J., Hayashi, I., & Koyama, K. 1997, *ApJ*, 474, 675  
 Weaver, K. A. & Reynolds, C. S. 1998, *ApJ*, 503, L39  
 Weaver, K. A., Krolik, J. H., & Pier, E. A. 1998, *ApJ*, 498, 213  
 Vaughan, S. & Edelson, R. 2001, *ApJ*, 548, 694  
 Veron, P., Lindblad, P. O., Zuiderwijk, E. J., Veron, M. P., & Adam, G. 1980, *A&A*, 87, 245  
 Zdziarski, A. A. & Grandi, P. 2001, *ApJ*, 551, 186

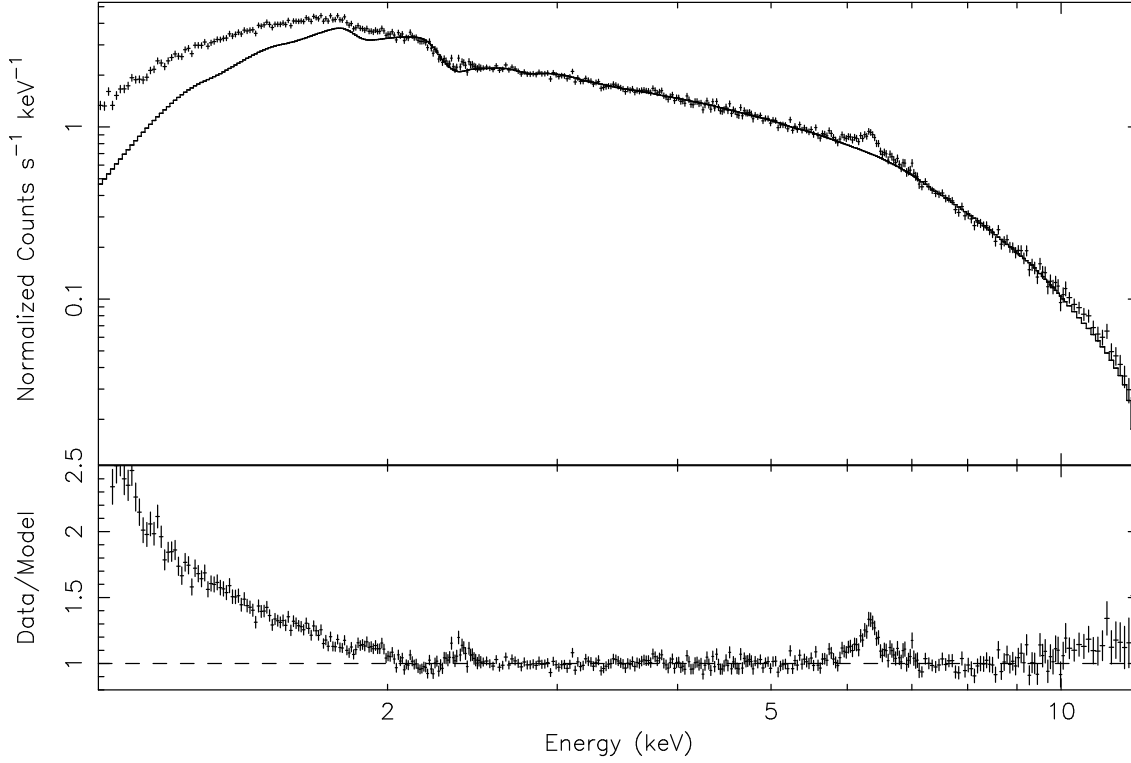


FIG. 1.— Ratio of combined PN data and the best-fit model derived by fitting an absorbed and red-shifted power-law to the observed data over the energy band of 2.5 – 10 keV but excluding the iron  $K\alpha$  region 5.0 – 7.5 keV band. A strong soft X-ray excess below 2 keV and an emission feature at  $\sim 6.4$  keV due to iron K-shell emission are seen clearly. Also seen is the excess emission over the power law above  $\sim 10$  keV.

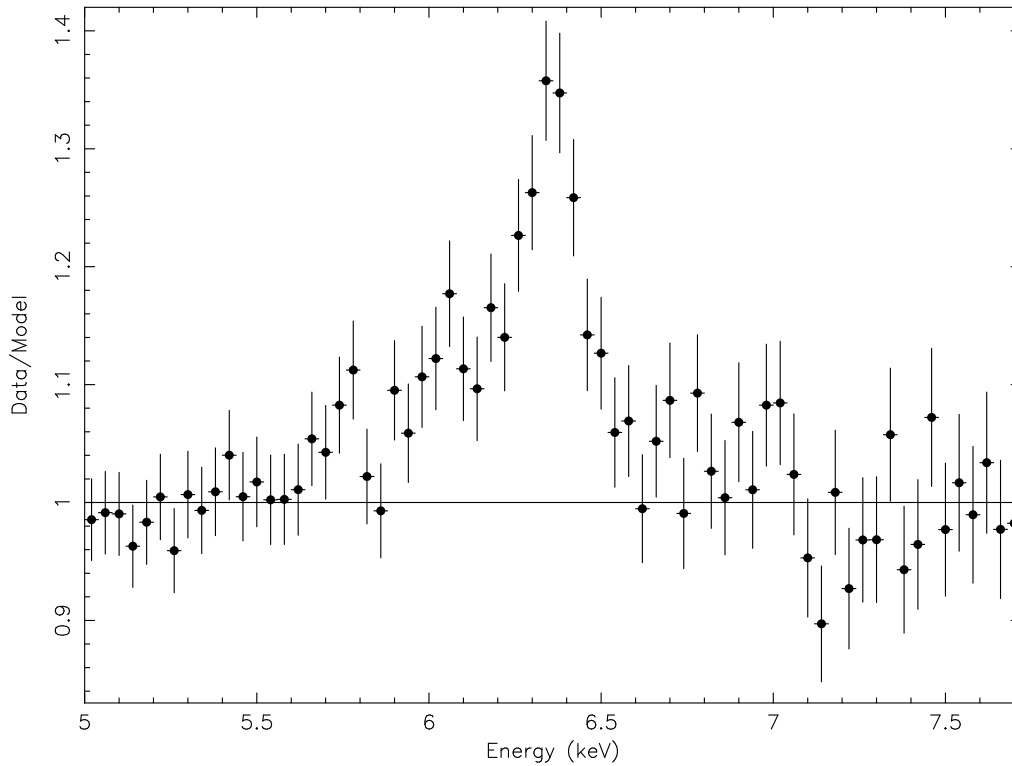


FIG. 2.— The Fe  $K\alpha$  region of the X-ray spectrum of MCG-5-23-16 shown as the ratio of the observed data of December 2001 and the best-fit power-law model. The best-fit power-law continuum was derived by using the data in the 2.5 – 5 keV and 7.5 – 10 keV bands. A strong and broad Fe  $K\alpha$  peaking at  $\sim 6.4$  keV is evident.

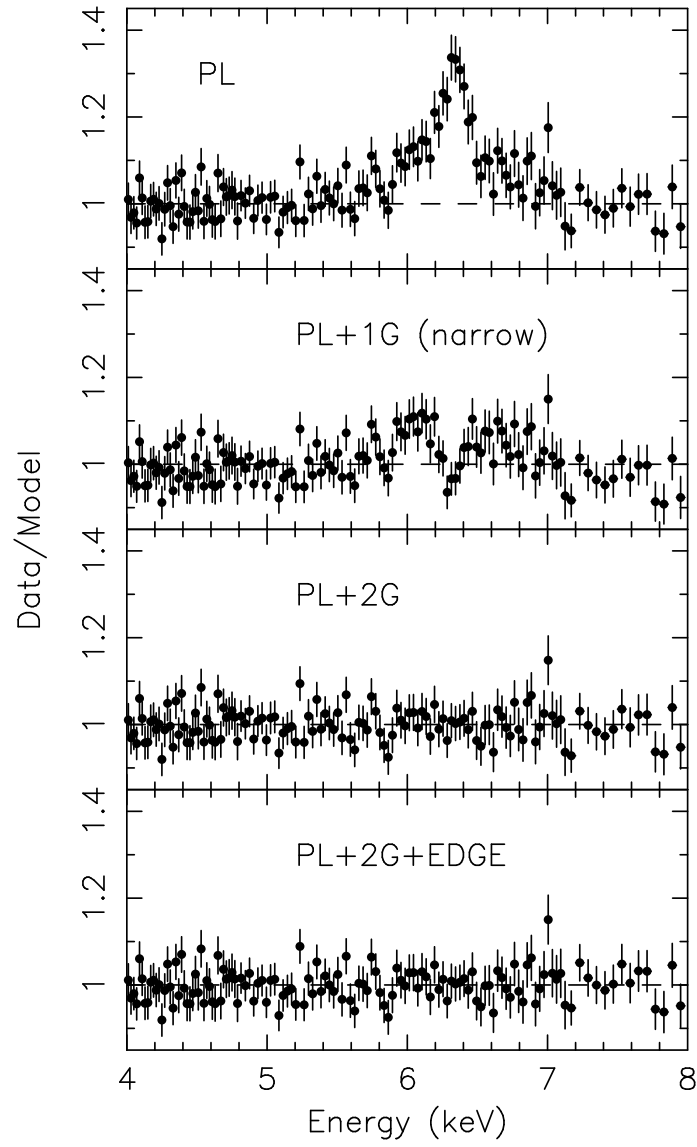


FIG. 3.— Ratios of combined PN data to the best-fit Gaussian models of the iron  $K\alpha$  line profile. From top, the best-fit models are (i) absorbed and red-shifted power law (PL), (ii) PL and a narrow Gaussian with  $\sigma = 0.01$  keV, (iii) PL and a combination of a narrow and a broad Gaussian, (iv) same as above but with an absorption edge at 7.1 keV.

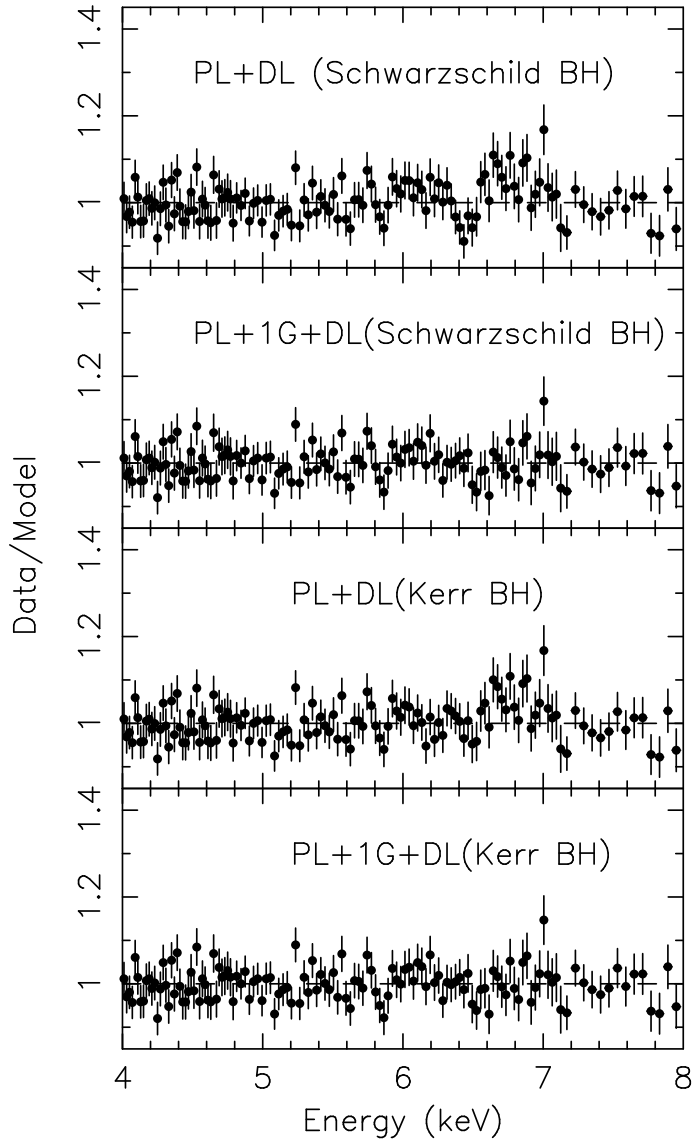


FIG. 4.— Ratios of combined PN data to the best-fit relativistic disk-line models for the iron  $K\alpha$  line profile. From the top, the best-fit models are (i) an absorbed and red-shifted power-law and a disk-line model for a Schwarzschild black hole, (ii) same as above with an addition of a narrow Gaussian line with  $\sigma = 0.01$  keV, (iii) PL and disk-line model for a Kerr black hole, (iv) same as above with the addition of a narrow Gaussian ( $\sigma = 0.01$  keV).

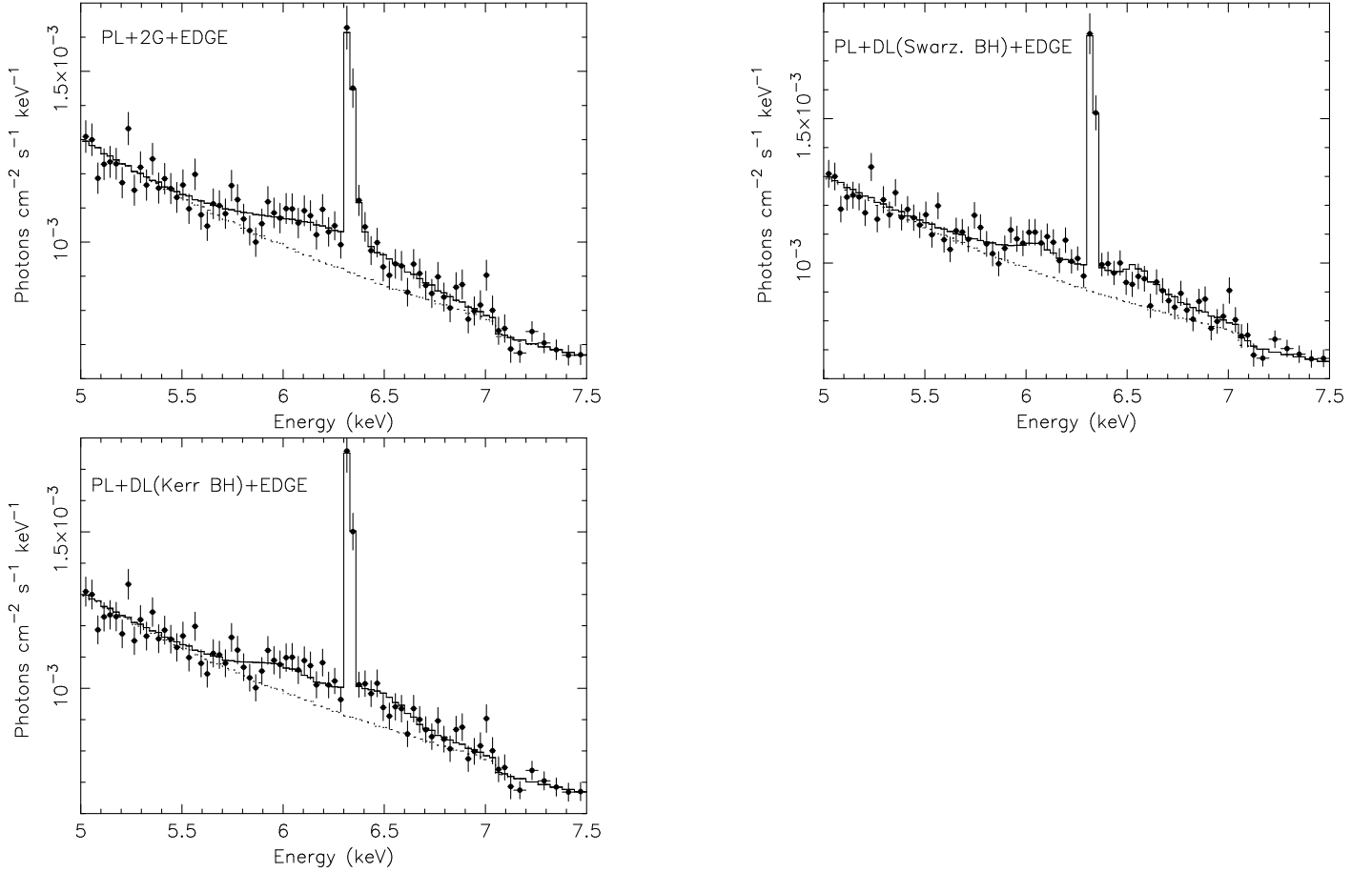


FIG. 5.— The average EPIC PN FeK $\alpha$  line profile of MCG-5-23-16 and the best-fit model consisting of (i) a narrow Gaussian and a broad Gaussian (top left panel), (ii) a combination of a narrow Gaussian and a line arising from an accretion disk around a Schwarzschild black hole (top right panel) or (iii) Kerr black hole (bottom panel).

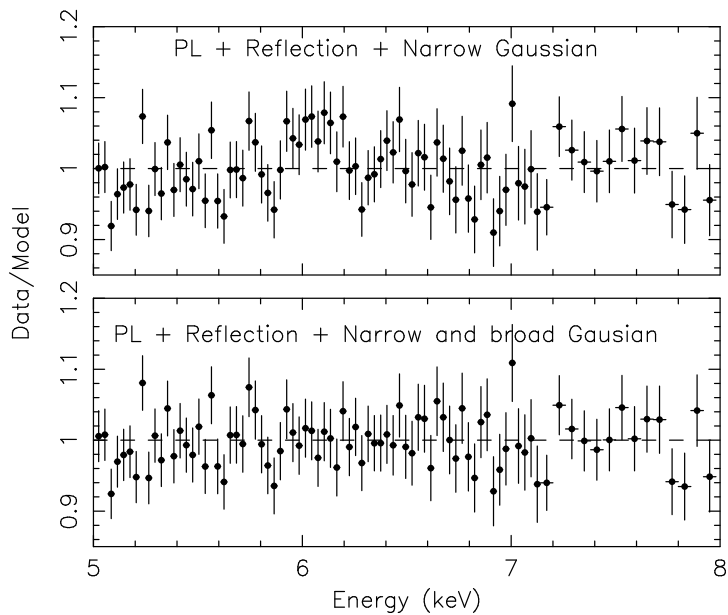


FIG. 6.— Ratio of the combined PN data to the best-fit reflection model with (i) a narrow Gaussian ( $\sigma = 100$  eV) for the iron K $\alpha$  emission (upper panel) and (ii) a narrow and a broad Gaussian for the iron K $\alpha$  emission.

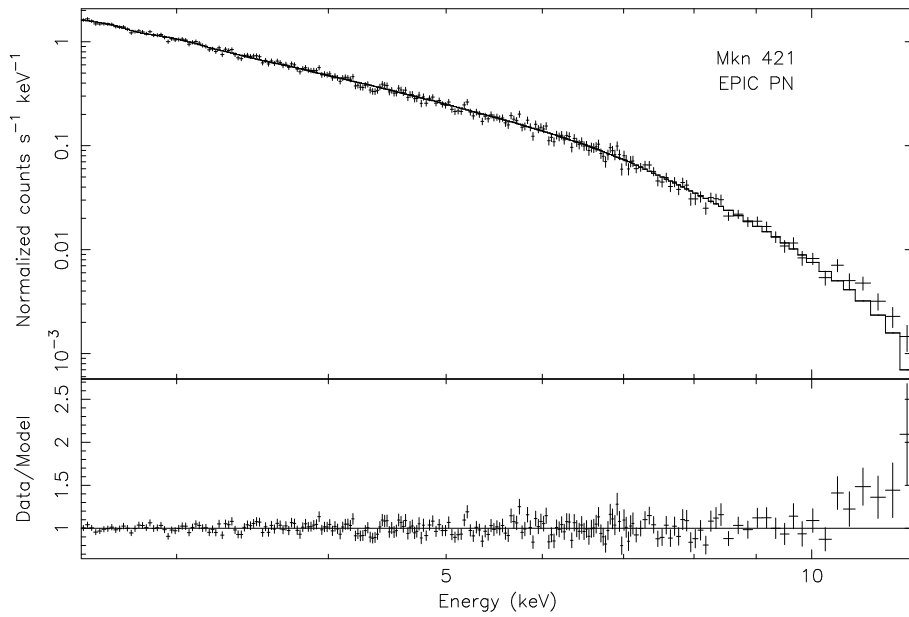


FIG. 7.— The EPIC PN spectrum of Mkn 421 and the best-fit power-law model over the 2.5 – 12 keV band. A clear excess over the best-fit power-law is seen at energies above  $\sim 10$  keV. This excess is similar within error to that seen in the PN spectrum of MCG-5-23-16.

TABLE 1  
BEST-FIT ABSORBED POWER-LAW MODEL PARAMETERS FOR MCG-5-23-16

Observation	Data <sup>a</sup>	Model <sup>b</sup>	$N_{\text{H}}^c$ $10^{22} \text{ cm}^{-2}$	$\Gamma_X$	$f_{obs}$	$f_{int}$	$\chi^2/dof$
2001 December	PN	PL	$1.67^{+0.19}_{-0.19}$	$1.66^{+0.03}_{-0.03}$	6.9	7.6	138.4/146
	MOS1	PL	$1.23^{+0.42}_{-0.42}$	$1.52^{+0.09}_{-0.09}$	5.7	6.1	169.8/161
	MOS2	PL	$1.56^{+0.43}_{-0.43}$	$1.55^{+0.10}_{-0.09}$	5.5	6.0	166.2/161
2001 May	PN+MOS1+MOS2	PL	$1.65^{+0.16}_{-0.15}$	$1.64^{+0.03}_{-0.03}$	6.0	6.5	478.0/472
	PN	PL	$1.93^{+0.28}_{-0.28}$	$1.75^{+0.04}_{-0.04}$	7.1	7.9	160.4/146
	MOS1	PL	$2.03^{+0.48}_{-0.48}$	$1.69^{+0.10}_{-0.10}$	6.4	7.2	182.9/161
	MOS2	PL	$1.89^{+0.48}_{-0.48}$	$1.70^{+0.11}_{-0.11}$	6.2	6.9	195.7/161
2001 Dec. + May	PN+MOS1+MOS2	PL	$2.09^{+0.22}_{-0.21}$	$1.77^{+0.04}_{-0.05}$	6.4	7.2	553/472
	PN	PL	$1.76^{+0.17}_{-0.17}$	$1.69^{+0.03}_{-0.03}$	7.0	7.7	123.6/158

<sup>a</sup>The data in the 2.5 – 10 keV were used.

<sup>b</sup>Simple red-shifted power-law modified by absorption

<sup>c</sup>Excess absorption intrinsic to the source apart from that due to the Galactic column of  $8.82 \times 10^{-20} \text{ cm}^{-2}$ .

TABLE 2  
BEST-FIT PARAMETERS OF THE TWO COMPONENT GAUSSIAN MODEL FOR THE IRON  $K\alpha$  EMISSION OF MCG-5-23-16

Parameter	PL					
	PN+MOS Dec. 2001		PN+MOS May 2001		Combined PN May and Dec. 2001	
	NO EDGE	EDGE	NO EDGE	EDGE	NO EDGE	EDGE
$\Gamma_X$	1.64	1.64	1.77	1.77	$1.69^{+0.03}_{-0.04}$	$1.65^{+0.05}_{-0.06}$
$N_{\text{H}}$	1.65	1.65	2.09	2.09	$1.75^{+0.16}_{-0.16}$	$1.60^{+0.22}_{-0.22}$
$E_N$	6.4	6.4	6.4	6.4	6.4	$6.39^{+0.02}_{-0.03}$
$\sigma_N$	0.01	0.01	0.01	0.01	0.01	0.01
$EW_N$	$48.0^{+7.8}_{-10.2}$	$52.3^{+6.6}_{-14.5}$	$49.1^{+13.2}_{-16.0}$	$46.1^{+11.2}_{-11.0}$	$35.3^{+9.6}_{-9.6}$	$35.2^{+9.6}_{-10.0}$
$E_B$	6.4	6.4	6.4	6.4	$6.32^{+0.07}_{-0.08}$	$6.32^{+0.09}_{-0.09}$
$\sigma_B$	$0.370^{+0.109}_{-0.076}$	$0.376^{+0.143}_{-0.074}$	$0.550^{+0.132}_{-0.110}$	$0.602^{+0.182}_{-0.138}$	$0.381^{+0.104}_{-0.087}$	$0.355^{+0.128}_{-0.060}$
$EW_B$	$91.5^{+21.5}_{-12.9}$	$92.6^{+18.4}_{-14.2}$	$177^{+38}_{-30}$	$189^{+44}_{-37}$	$114^{+21.0}_{-21.4}$	$96.4^{+31.6}_{-30.7}$
$E_{edge}$	–	7.1	–	7.1	–	7.1
$\tau$	–	$0.02^{+0.02}_{-0.02p}$	–	$0.02^{+0.03}_{-0.02p}$	–	$0.03^{+0.04}_{-0.02}$
$\chi^2_{min}$	727.2	722.9	783.8	782.5	186.7	184.0
dof	697	696	703	702	232	231

TABLE 3  
RESULTS FOR RELATIVISTIC DISK-LINE FITS TO THE COMBINED PN DATA

Parameter	Schwarzschild geometry		Kerr geometry	
	NO EDGE	EDGE	NO EDGE	EDGE
$\Gamma_X$	$1.68 \pm 0.02$	$1.68 \pm 0.02$	$1.68 \pm 0.03$	$1.65^{+0.05}_{-0.10}$
Normalization <sup>a</sup>	$0.021 \pm 0.001$	$0.021 \pm 0.001$	$0.021 \pm 0.001$	$0.021 \pm 0.001$
$N_H (\times 10^{22} \text{ cm}^{-2})$	$1.72^{+0.12}_{-0.16}$	$1.72^{+0.14}_{-0.17}$	$1.72^{+0.18}_{-0.21}$	$1.62^{+0.17}_{-0.17}$
$E_N$ (keV)	6.4	6.4	6.4	6.4
$\sigma_N$ (eV)	100	100	100	100
$EW_N$ (eV)	$43.5^{+9.6}_{-9.6}$	$44.7^{+7.4}_{-7.0}$	$38.0^{+9.3}_{-9.6}$	$38.5^{+9.3}_{-9.6}$
$E_D$ (keV)	$6.31^{+0.06}_{-0.25}$	$6.30^{+0.07}_{-0.23}$	$6.29^{+0.09}_{-0.12}$	$6.30^{+0.09}_{-0.12}$
$q$	$1.81^{+0.40}_{-0.37}$	$1.81^{+0.41}_{-0.38}$	$1.75^{+0.38}_{-0.55}$	$1.73^{+0.36}_{-0.61}$
$r_i/r_g$	6	6	1.23	1.23
$r_o/r_g$	400	400	400	400
$i$	$46.3^{+3.4}_{-3.8}$	$46.0^{+2.5}_{-3}$	$47.4^{+6.9}_{-6.7}$	$47.9^{+9.9}_{-7.1}$
$EW_D$ (eV)	$119^{+31}_{-23}$	$128^{+23}_{-22}$	$118^{+28}_{-25}$	$116^{+27}_{-25}$
$E_{edge}$ (keV)	–	7.1	–	7.1
$\tau$	–	$0.010^{+0.021}_{-0.0p}$	–	$0.03^{+0.08}_{-0.03p}$
$\chi^2/dof$	190.7/232	190.4/231	191.1/232	188.7/231

<sup>a</sup>Power-law normalization at 1 keV in units of photons  $\text{keV}^{-1} \text{s}^{-1} \text{cm}^{-2}$ .

TABLE 4  
BEST-FIT PARAMETERS OF A REFLECTION MODEL FOR THE CONTINUUM AND GAUSSIAN MODEL FOR THE IRON  $K\alpha$  EMISSION OF MCG-5-23-16

Parameter	PL + Reflection			
	Reflection parameters varied		Reflection parameters fixed <sup>a</sup>	
	Single Gaussian	Double Gaussian	Single Gaussian	Double Gaussian
$N_H (\times 10^{22} \text{ cm}^{-2})$	$1.8^{+0.1}_{-0.2}$	$1.75^{+0.06}_{-0.08}$	$1.75^{+0.08}_{-0.15}$	$1.67^{+0.08}_{-0.05}$
$\Gamma_X$	$1.85^{+0.03}_{-0.05}$	$1.78^{+0.02}_{-0.02}$	$1.68^{+0.03}_{-0.03}$	$1.68^{+0.05}_{-0.02}$
$E_{fold}$	200 keV	200 keV	157 keV	157 keV
$R$	$2.5^{+0.3}_{-0.4}$	$1.7^{+0.2}_{-0.2}$	0.54	0.54
$i$	$60^\circ$	$60^\circ$	$60^\circ$	$60^\circ$
$E_N$	$6.37^{+0.03}_{-0.02}$	6.4	6.4	6.4
$\sigma_N$ (eV)	0.01	0.01	0.01	0.01
$EW_N$ (eV)	$52.0^{+6.9}_{-7.7}$	$43.2^{+6.1}_{-11.4}$	$62.0^{+9.3}_{-6.4}$	$34.5^{+10.2}_{-11.4}$
$E_B$	–	$6.20^{+0.10}_{-0.12}$	–	$6.28^{+0.08}_{-0.08}$
$\sigma_B$	–	$0.18^{+0.09}_{-0.12}$	–	$0.31^{+0.12}_{-0.09}$
$EW_B$	–	$29.2^{+33.5}_{-13.8}$	–	$83.9^{+12.3}_{-22.6}$
$\chi^2_{min}$	224.4	204.3	234.6	184.3
$dof$	269	267	236	233

<sup>a</sup>Relative reflection  $R$  and cut-off energy  $E_C$  were fixed at the values derived from the *BeppoSAX* observations (Risaliti 2002).